

# Leading twist nuclear shadowing and suppression of hard coherent diffraction in proton-nucleus scattering

V. Guzey

*Institut für Theoretische Physik II,*

*Ruhr-Universität Bochum, D-44780 Bochum, Germany*<sup>\*</sup>

M. Strikman

*Department of Physics, Pennsylvania State University, University Park, PA 16802, USA*<sup>†</sup>

## Abstract

We use the theory of leading twist shadowing to develop a method for the calculation of hard leading twist coherent diffraction in hadron-nucleus processes. We demonstrate that soft multiple rescatterings lead to the factorization breaking of hard diffraction in proton-nucleus scattering, which is larger than in hadron-nucleon scattering. At the LHC and RHIC kinematics, we compare the contribution of hard diffraction into two jets to the e.m. contribution, when the two-jet diffractive final state is produced by the coherent nuclear Coulomb field. We study the  $x_{IP}$ ,  $\beta$  and  $A$ -dependence of the ratio of the two effects,  $R$ . We demonstrate that in proton-heavy nucleus hard coherent diffraction at the LHC,  $R$  is small, which offers a clean method to study hard photon-proton scattering at the energies exceeding the HERA energies by the factor of ten. On the other hand, the use of lighter nuclei, such as  $^{40}\text{Ca}$ , will allow to study the screened nuclear diffractive parton distribution. Moreover, a comparison of the dijet diffractive production to the heavy-quark-jet diffractive production will estimate the screened nuclear diffractive gluon PDF, which will be measured in nucleus-nucleus ultraperipheral collisions at the LHC.

PACS numbers: 24.85.+p,25.40.Ep,13.87.-a

---

<sup>\*</sup>vadim.guzey@tp2.ruhr-uni-bochum.de

<sup>†</sup>strikm@phys.psu.edu

## I. INTRODUCTION

The phenomenon of hard diffraction, which was first discovered at the SPC proton-antiproton collider at CERN [1], was further studied at HERA in electron-proton collisions, see e.g. [2]. It was realized that hard diffractive processes in deep inelastic scattering (DIS) can be treated similarly to inclusive DIS due to the QCD factorization theorem [3]. In general, diffractive processes play an important role as a way of probing the strength of the underlying interaction. In particular, the ratio of the diffractive and total cross sections approaches 1/2 in the high-energy limit when the interaction becomes completely absorptive.

The studies at Tevatron have demonstrated that there is a significant suppression of hard diffractive processes as compared to expectations based on the application of the factorization theorem [4, 5]. This can be semi-quantitatively understood as due to the absorptive effects associated with multi-Pomeron exchanges, which make the gap survival very unlikely for the case of hadronic collisions, see e.g. [6]. The effect is primarily due to the negligible probability to avoid inelastic interactions for the scattering at small impact parameters [7].

Turning to DIS with nuclear targets, it is possible to express nuclear shadowing of nuclear parton distribution functions (PDFs) at sufficiently low values of Bjorken  $x$  through the nucleon diffractive PDFs [8] – for a recent summary, see [9]. Recently we extended the leading twist theory of nuclear shadowing to diffractive DIS processes. We calculated diffractive PDFs for nuclei at small  $x$ , expressing them through nucleon diffractive PDFs and using the same approximations as in the study of nuclear shadowing [10]. In this work, we make a next step and study hard diffraction in proton-nucleus collisions. The main theoretical issue, which we address, is to what extent the absorptive effects will modify hard diffraction in hadron-nucleus collisions compared to the hadron-nucleon case.

The paper consists of two parts. In Sect. II, we derive general expressions for the nuclear modifications of hard diffraction in  $pA$  scattering. We demonstrate that because of multiple soft rescatterings, hard diffractive processes like production of two jets, heavy flavors, etc. are suppressed at the LHC and RHIC energies stronger than soft inelastic diffraction, which in turn is expected to be strongly suppressed [11, 12, 13].

In Sect. III, we compare the contribution of hard coherent diffraction into two jets (including heavy quark jets) to the e.m contribution, when the final state containing two hard jets is produced by the coherent nuclear Coulomb field. We demonstrate that the e.m contribution

dominates proton-Pb scattering at the LHC, which provides essentially a background-free method to study very high-energy  $\gamma p$  scattering at the LHC through ultraperipheral proton-nucleus scattering. We show that using lighter nuclei, which do not produce a strong flux of equivalent photons, one can study screened nuclear diffractive PDFs. In this case, a comparison of the dijet diffractive production to the heavy-quark-jet diffractive production will measure the nuclear screened diffractive gluon PDF. It can be compared to the nuclear diffractive PDFs, which will be measured in nucleus-nucleus ultraperipheral collisions at the LHC.

The conclusion about the dominance of the hard diffractive mechanism over the e.m. one, when light nuclei are used, also holds in the RHIC kinematics.

Our results are also valid for the diffraction in resolved photon-nucleus interactions. Since in this case several other effects are also important, we will discuss hard diffraction in  $\gamma A$  interactions in a separate publication.

## II. SUPPRESSION FACTOR FOR HARD DIFFRACTION

We consider an example of hard coherent diffraction of protons on nuclei,  $p + A \rightarrow 2 \text{jets} + X + A$ , where the final diffractive state contains two jets (including jets containing heavy quarks), whose invariant mass provides a hard scale, and a soft diffractive component  $X$ .

The suppression factor can be derived using the following lines of reasoning. First, in the case of soft diffraction on heavy nuclei, the diffractive cross section receives the dominant contribution from color (cross section) fluctuations in the projectile proton, which are close to the average size, such that the effect of the fluctuations can be retained with the interaction with only one target nucleon [11]. This approximation agrees well with available fixed-target data, see a review in [12]. Second, we demonstrated in [13] that at the LHC energies, the color fluctuations, which contribute to the diffraction cross section, are further suppressed, which strengthens the approximation that the proton-nucleus diffractive cross section is determined by the set of the rescattering diagrams where the incoming proton dissociates in one vertex only.

Third, a straightforward analysis of the Glauber series shows that the combinatoric factor for the  $k$ -fold scattering in the considered case differs from the elastic scattering case by the

factor  $k$  (we have  $1/(k-1)!$  instead of  $1/k!$ ), see e.g. [14]. As a result, the proton-nucleus diffractive amplitude at a given impact parameter can be conveniently written through the derivative with respect to the total proton-nucleon cross section  $\sigma_{\text{tot}}$  of the proton-nucleus elastic amplitude:

$$\begin{aligned} A_{\text{diff}}^{p+A \rightarrow X+A}(b) &= 4\pi A_{\text{diff}}^{p+N \rightarrow X+N}(t=0) \frac{\partial A_{\text{el}}^{p+A \rightarrow p+A}(b)}{\partial \sigma_{\text{tot}}} \\ &= 4\pi A_{\text{diff}}^{p+N \rightarrow X+N}(t=0) \frac{\partial \left(1 - \exp(-T_A(b) \frac{\sigma_{\text{tot}}}{2})\right)}{\partial \sigma_{\text{tot}}} \\ &= 2\pi A_{\text{diff}}^{p+N \rightarrow X+N}(t=0) T_A(b) \exp\left(-T_A(b) \frac{\sigma_{\text{tot}}}{2}\right), \end{aligned} \quad (1)$$

where  $A_{\text{diff}}^{p+N \rightarrow X+N}(t=0)$  is the proton-nucleon diffraction dissociation amplitude at  $t=0$ ;  $T_A(b) = \int dz \rho_A(b, z)$  and  $\rho_A(b, z)$  is the nuclear density;  $\sigma_{\text{tot}}$  is the total hadron-nucleon cross section. The  $2\pi$  factor comes from the Fourier transform from the impact parameter to the momentum representation.

In the case of hard diffraction we also need to take into account the suppression of nuclear diffractive PDFs. The corresponding suppression factor  $T^{\text{hard}}$  is given by [10]

$$T^{\text{hard}} = \exp\left(-T_A(b) \frac{\sigma_{\text{eff}}}{2}\right), \quad (2)$$

where  $\sigma_{\text{eff}}$  is the effective rescattering cross section for the diffractively produced final state

$$\sigma_{\text{eff}} = \sigma_{\text{eff}}^j(x, Q_0^2) = \frac{16\pi}{f_{j/N}(x, Q_0^2)(1+\eta^2)} \int dx_{IP} f_{j/N}^{D(4)}(\beta, Q_0^2, x_{IP}, t \approx 0), \quad (3)$$

where  $j$  is the parton flavor;  $f_{j/N}$  is the nucleon PDF;  $f_{j/N}^{D(4)}$  is the proton diffractive PDF;  $\eta$  is the ratio of the real to imaginary parts of the diffractive scattering amplitude. Note that  $\sigma_{\text{eff}}$  depends on the parton flavor, Bjorken  $x$  and the resolution scale  $Q_0^2$ .

As explained in [9], the correct procedure of the evaluation of leading twist nuclear shadowing is the following. First, one calculates the shadowing correction to inclusive or diffractive nuclear PDFs at the initial resolution scale  $Q_0^2$  using  $\sigma_{\text{eff}}$  of Eq. (3). Then, one uses the result as an input for DGLAP evolution of the nuclear PDFs to higher scales  $Q^2$ . The use of Eq. (3) at any  $Q^2$  scale, i.e. the use of the  $Q^2$ -dependent  $\sigma_{\text{eff}}$ , leads to correct pQCD evolution only in the case of small nuclear shadowing. Another example, where it is justified to use the  $Q^2$ -dependent  $\sigma_{\text{eff}}$ , is the case of the suppression of hard diffraction considered in this work. Indeed, since the suppression factor is defined by the sum  $\sigma_{\text{tot}} + \sigma_{\text{eff}}$ , where  $\sigma_{\text{tot}}$  is of the order of 100 mb at the LHC energies and  $\sigma_{\text{eff}} < \sigma_{\text{tot}}$ , the effect of QCD

evolution is numerically small. This is true to a lesser degree for the RHIC energy, where  $\sigma_{\text{tot}}$  is smaller.

Thus, introducing the suppression factor  $T^{\text{hard}}$  into Eq. (1), squaring the amplitude and integrating it over the impact parameter, we obtain the final expression for the proton-nucleus diffractive cross section

$$\sigma_{\text{diff}}^{p+A \rightarrow 2\text{jets}+X+A} = 4\pi \left( \frac{d\sigma_{\text{diff}}^{p+p \rightarrow 2\text{jets}+X+p}}{dt} \right)_{t=0} \int d^2b T_A^2(b) \exp [-(\sigma_{\text{tot}} + \sigma_{\text{eff}})T_A(b)] . \quad (4)$$

Note that we related the elementary diffractive dissociation amplitude to the corresponding differential cross section,  $|A_{\text{diff}}^{p+N \rightarrow X+N}(t = 0)|^2 = 1/\pi \sigma_{\text{diff}}^{p+p \rightarrow 2\text{jets}+X+p}/dt(t = 0)$ . Also, in Eq. (4) we neglected the effect of the non-zero coherence length, which significantly simplified the numerical analysis of the equation.

We can interpret our final expression in a somewhat different way. Equation (4) is convolution of the diffractive PDFs in a nucleus at a given  $b$  with the probability of absence of inelastic soft interactions at a given impact parameter, which is given by the factor  $\exp(-\sigma_{\text{tot}} T_A(b))$ .

In more detail, the derivation proceeds as follows. Imposing the condition that a hard collision is possible, we also take into account the condition that the diffractive PDF is screened. The screening factor  $T^{\text{hard}}$  can be calculated in the quasi-eikonal approximation using the effective cross section for the interaction in the gluon or quark induced-diffraction and is given by Eq. (2). In order to simultaneously include the suppression of the hard diffractive PDFs and screening due to soft inelastic scattering off other nucleons, we combine the two suppression effects – this is straightforward due to the exponential structure of the dependence on  $\sigma_{\text{eff}}$  and  $\sigma_{\text{tot}}$ . The final expression for the diffractive cross section is given by Eq. (4).

We are interested in the suppression of hard diffraction due to nuclear shadowing (rescattering or screening) effects as compared to the proton target. In order to quantify the suppression with respect to the total cross section, one can study the following double ratio

$$\lambda_1 = \frac{\sigma^{p+A \rightarrow 2\text{jets}+X+A}}{\sigma_{\text{tot}}^{pA}} \Big/ \frac{\sigma^{p+p \rightarrow 2\text{jets}+X+p}}{\sigma_{\text{tot}}^{pp}} . \quad (5)$$

Wishing to examine the suppression of hard diffraction with respect to diffraction dissociation (inelastic diffraction), one can examine the following double ratio

$$\lambda_2 = \frac{\sigma^{p+A \rightarrow 2\text{jets}+X+A}}{\sigma_{\text{DD}}^{pA}} \Big/ \frac{\sigma^{p+p \rightarrow 2\text{jets}+X+p}}{\sigma_{\text{DD}}^{pp}} . \quad (6)$$

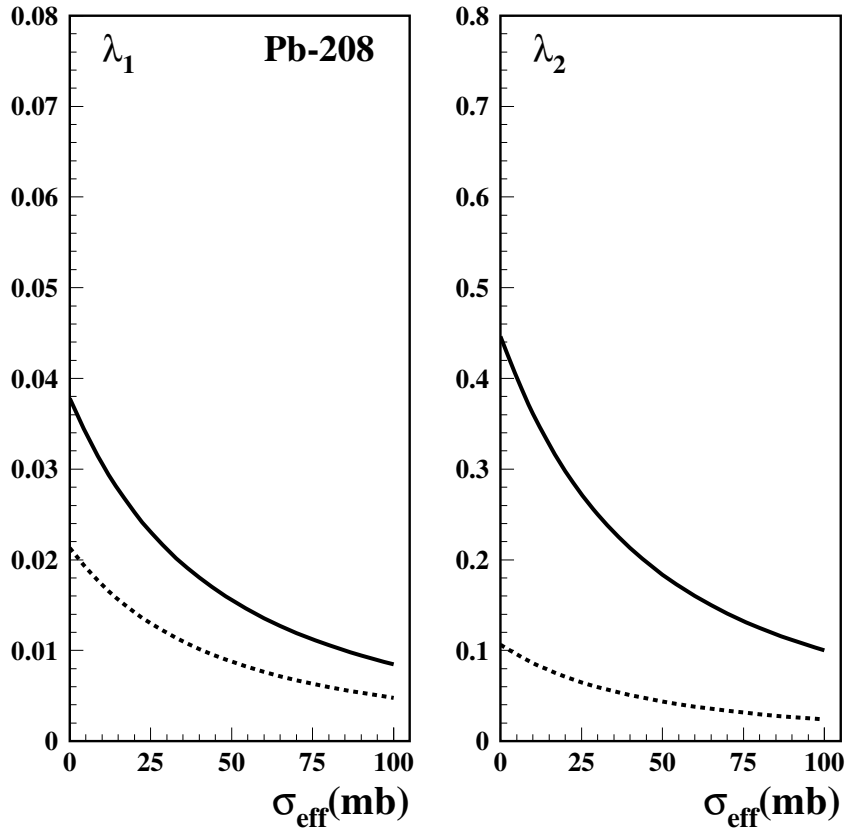


FIG. 1: The suppression factors  $\lambda_1$  and  $\lambda_2$  of Eqs. (5) and (6) for  $^{208}\text{Pb}$  in the LHC (solid curves) and RHIC (dotted curves) kinematics.

The  $\lambda_1$  and  $\lambda_2$  suppression factors for  $^{208}\text{Pb}$  at the LHC energy of  $\sqrt{s} = 8800$  GeV per nucleon [15] (solid curves) and at the RHIC energy of  $\sqrt{s} = 200$  GeV per nucleon (dotted curves) as functions of  $\sigma_{\text{eff}}$  are presented in Fig. 1. The  $A$ -dependence of  $\lambda_1$  and  $\lambda_2$  at two typical values of  $\sigma_{\text{eff}}$ ,  $\sigma_{\text{eff}} = 25$  and  $40$  mb (see [9]), is presented in Fig. 2.

The small values of  $\lambda_1$  and  $\lambda_2$  in Figs. 1 and 2 mean that in hadron-nucleus scattering, hard diffraction constitutes a much small fraction of the total and diffractive dissociation cross sections than in proton-proton scattering. This suppression of hard diffraction is substantially stronger than the suppression of soft inelastic diffraction, which is itself strongly suppressed at the LHC [13].

The fact that the suppression factors  $\lambda_1$  and  $\lambda_2$  for a given nucleus in Figs. 1 and 2

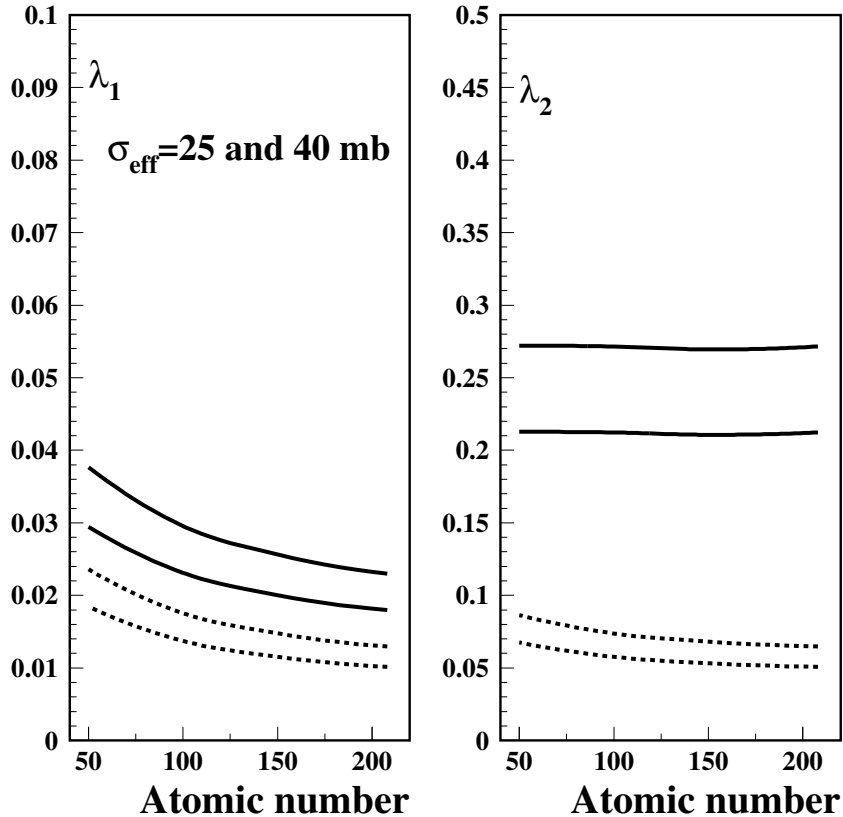


FIG. 2: The suppression factors  $\lambda_1$  and  $\lambda_2$  of Eqs. (5) and (6) at  $\sigma_{\text{eff}} = 25$  and  $40$  mb in the LHC (solid curves) and RHIC (dotted curves) kinematics. The curves corresponding to  $\sigma_{\text{eff}} = 25$  mb lie above the curves calculated with  $\sigma_{\text{eff}} = 40$  mb.

are smaller for the RHIC energy than for the LHC can be explained by Eqs. (11). At the considered energies, the integral over  $d^2b$  does not significantly change by increasing  $\sigma_{\text{tot}}$  and is predominantly determined by the nuclear size. Therefore, the energy variation of  $\lambda_1$  and  $\lambda_2$  is defined by the  $\bar{B}\sigma_{\text{tot}}^{pp}/\sigma_{\text{tot}}^{pA}$  and  $\bar{B}\sigma_{\text{DD}}^{pp}/\sigma_{\text{DD}}^{pA}$  factors, respectively, which are larger in the LHC kinematics.

As can be seen from Fig. 2, the  $A$ -dependence of  $\lambda_1$  and  $\lambda_2$  at the both values of  $\sigma_{\text{eff}}$  is rather weak.

In our numerical analysis, we used the following inputs. The total ( $\sigma_{\text{tot}}^{pA}$ ) and diffractive differential ( $\sigma_{\text{diff}}^{pA}$ ) proton-nucleus cross sections at the LHC and RHIC energies are taken from the calculation of [13] which is presented in Fig. 3 of that paper.

The diffractive dissociation proton-proton cross section ( $\sigma_{\text{DD}}^{pp}$ ) is estimated assuming the exponential  $t$ -dependence for the differential cross section after the integration over diffractive masses and using energy-dependent cross section fluctuations [13]

$$\sigma_{\text{DD}}^{pp} = \frac{1}{\bar{B}} \left( \frac{d\sigma_{\text{DD}}^{pp}}{dt} \right)_{t=0} = \frac{1}{16\pi\bar{B}} (\langle \sigma^2 \rangle - \langle \sigma \rangle^2) = \frac{1}{16\pi\bar{B}} \omega_\sigma \langle \sigma \rangle^2 = \frac{1}{16\pi\bar{B}} \omega_\sigma (\sigma_{\text{tot}}^{pp})^2. \quad (7)$$

In Eq. (7),  $\bar{B}$  is the average slope of the soft diffractive dissociation cross section, which was estimated as follows. Starting from the common Regge-type parameterization of the single diffractive cross section,

$$s \frac{d^2\sigma_{\text{diff}}}{dM_X^2 dt} \propto \left( \frac{s}{M_X^2} \right)^{1+\epsilon} \exp \left( [b_0 + 2\alpha' \ln(s/M_X^2)] t \right), \quad (8)$$

where  $M_X$  is the produced diffractive mass;  $\alpha' = 0.25 \text{ GeV}^{-2}$ ;  $\epsilon \approx 0$  [5] and  $b_0 \approx 4.6 \text{ GeV}^{-2}$ , one can readily estimate  $\bar{B}$ , which we define as

$$\bar{B} = \frac{\int_{1.4 \text{ GeV}^2}^{0.15s} dM_X^2 \left( \frac{d^2\sigma_{\text{diff}}}{dM_X^2 dt} \right)_{t=0}}{\int_{1.4 \text{ GeV}^2}^{0.15s} dM_X^2 \int_{-1 \text{ GeV}^2}^0 dt \left( \frac{d^2\sigma_{\text{diff}}}{dM_X^2 dt} \right)}. \quad (9)$$

Note that we used the observation of [5] that for diffraction at high energies,  $\epsilon$  is effectively close to zero.

In Eq. (7),  $\omega_\sigma$  is the parameter, which controls the magnitude of cross section fluctuations. Numerically,  $\omega_\sigma \approx 0.3$  at RHIC and  $\omega_\sigma \approx 0.1$  at the LHC, see the discussion and references in [13]. The parameterization of the total proton-proton cross section is taken from [17]. A direct evaluation of Eqs. (9) and (7) gives

$$\begin{aligned} \bar{B} &= 7.34 \text{ GeV}^{-2}, \quad \sigma_{\text{DD}}^{pp} = 5.55 \text{ mb} \quad \text{RHIC}, \\ \bar{B} &= 8.85 \text{ GeV}^{-2}, \quad \sigma_{\text{DD}}^{pp} = 5.16 \text{ mb} \quad \text{LHC}. \end{aligned} \quad (10)$$

For the hard diffractive cross section, we also assumed an exponential  $t$ -dependence with the slope  $\bar{B}$  of Eq. (10). Therefore, the ratios  $\lambda_1$  and  $\lambda_2$  become

$$\begin{aligned} \lambda_1 &= 4\pi\bar{B} \int d^2b T_A^2(b) \exp [-(\sigma_{\text{tot}} + \sigma_{\text{eff}})T_A(b)] \left( \frac{\sigma_{\text{tot}}^{pp}}{\sigma_{\text{tot}}^{pA}} \right), \\ \lambda_2 &= 4\pi\bar{B} \int d^2b T_A^2(b) \exp [-(\sigma_{\text{tot}} + \sigma_{\text{eff}})T_A(b)] \left( \frac{\sigma_{\text{DD}}^{pp}}{\sigma_{\text{DD}}^{pA}} \right). \end{aligned} \quad (11)$$

Finally, the  $T_A(b)$  factor is evaluated using a simple model for the nuclear density  $\rho_A$ , see e.g. Appendix A of [9].

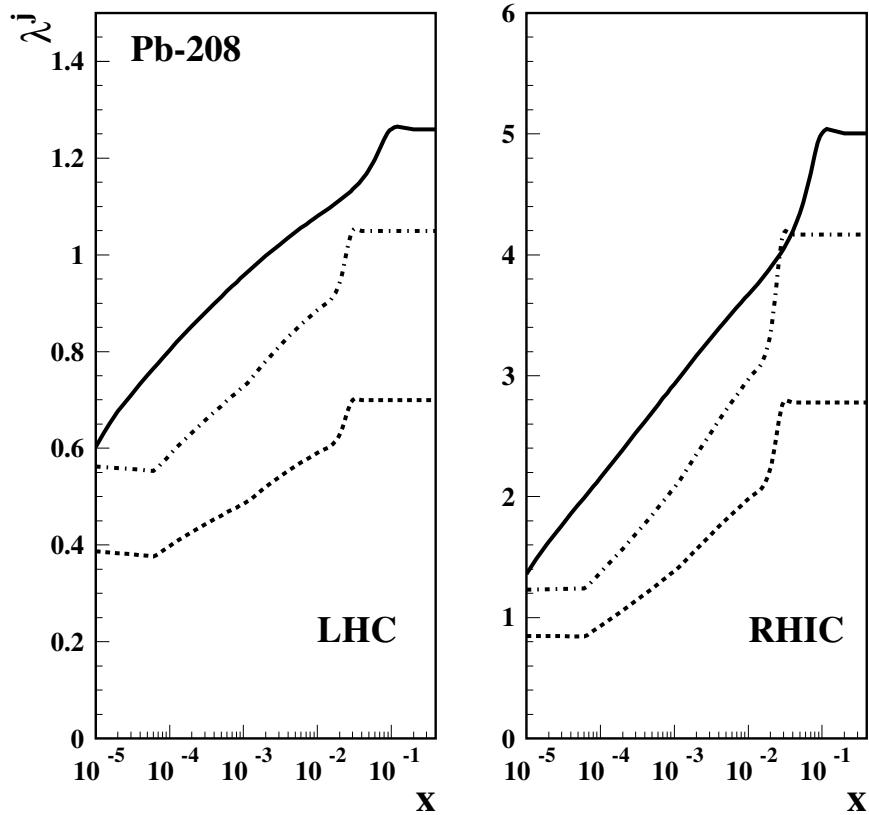


FIG. 3: The suppression factor  $\lambda^j$  of Eq. (12) as a function of Bjorken  $x$  at  $Q^2 = 4$  GeV $^2$  in the LHC ( $\sqrt{s} = 8.8$  TeV) and RHIC ( $\sqrt{s} = 200$  GeV) kinematics. The solid curve correspond to the sea  $u$ -quark; the dashed curve corresponds to the gluons in the low shadowing scenario; the dot-dashed curve corresponds to the gluons in the high shadowing scenario.

Equation (4) can be used to estimate the suppression of effective (including shadowing effects due to the soft rescattering) nuclear diffractive PDFs ( $\tilde{f}_{j/A}^{D(3)}$ ) compared to the free effective nucleon diffractive PDFs ( $\tilde{f}_{j/N}^{D(3)}$ ). The effective (screened) diffractive PDFs take into account factorizations breaking, which for the proton-nucleus diffraction arises as a suppression due to the soft rescattering [the presence of  $\sigma_{\text{tot}}$  in Eq. (12)] and which for the proton-proton diffraction is observed experimentally and is introduced phenomenologically by the factor  $r_h$  in Eq. (13).

The resulting suppression factor  $\lambda^j$  depends on the parton flavor  $j$ , Bjorken  $x$  and  $Q^2$  via the dependence of  $\sigma_{\text{eff}}^j$  on  $j$ ,  $x$  and  $Q^2$  and the dependence of the diffractive slope  $B_{\text{diff}}^j$  on  $j$

and  $x$ :

$$\lambda^j(x, Q^2) \equiv \frac{\tilde{f}_{j/A}^{D(3)}(\beta, x_{IP}, Q^2)}{\tilde{f}_{j/N}^{D(3)}(\beta, x_{IP}, Q^2)} = B_{\text{diff}}^j(4\pi) \int d^2 b T_A^2(b) \exp \left[ -(\sigma_{\text{tot}} + \sigma_{\text{eff}}^j(x, Q^2)) T_A(b) \right]. \quad (12)$$

The diffractive slope  $B_{\text{diff}}^j$  appeared after the conversion of  $\tilde{f}_{j/N}^{D(4)}(\beta, Q^2, x_{IP}, t \approx 0)$  to  $\tilde{f}_{j/N}^{D(3)}(\beta, Q^2, x_{IP})$ , see Eq. 10 of [9] and compare to Eq. (11). Note that while the diffractive PDFs depend separately on  $\beta$  and  $x_{IP}$ , the suppression factor  $\lambda^j(x, Q^2)$  depends only on their product  $x = \beta x_{IP}$  in our approach. Note that for the LHC energies, where  $\sigma_{\text{tot}}$  is of the order of 100 mb, the dependence of the suppression on  $\sigma_{\text{eff}}$  is rather weak. Therefore, a rather significant difference in  $\sigma_{\text{eff}}^j$  between the quark and gluon channels leads to a very small variation of  $\lambda^j$  (the main effect causing the difference in  $\lambda^j$  for different parton flavors is the different  $B_{\text{diff}}^j$ ). Hence, for a given parton flavor,  $\lambda^j$  remains practically the same at given  $x$  and  $x_{IP}$  for different  $Q^2$  hard scales.

In the numerical analysis of Eq. (12), we used the results of [9]. For the diffractive slopes, we used  $B_{\text{diff}}^{\text{quark}} = 7.2 \text{ GeV}^{-2}$  for quarks and  $B_{\text{diff}}^{\text{gluon}} = 4 + 0.2 \ln(10^{-3}/x) \text{ GeV}^{-2}$  and  $B_{\text{diff}}^{\text{gluon}} = 6 + 0.25 \ln(10^{-3}/x) \text{ GeV}^{-2}$  for gluons for  $x \leq 10^{-3}$ . For  $x > 10^{-3}$ , the used gluon slopes are 4 and 6  $\text{GeV}^{-2}$ , respectively. The two gluons slopes correspond to the low and high gluon shadowing scenarios considered in [9], which takes into account the uncertainty of theoretical predictions for nuclear shadowing in the gluon channel. The quark and gluon  $\sigma_{\text{eff}}^j$  at  $Q^2 = 4 \text{ GeV}^2$  are given in Fig. 4 of [9].

Figures 3 and 4 present the results of our calculations of  $\lambda^j$  in the RHIC and LHC kinematics. Figure 3 gives  $\lambda^j$  as a function of Bjorken  $x$  at  $Q^2 = 4 \text{ GeV}^2$ . The solid curves correspond to the  $\bar{u}$ -quark; the dashed curves correspond to the gluons in the low shadowing scenario; the dot-dashed curves correspond to the gluons in the high shadowing scenario. Despite the fact that  $\lambda^i(x, Q^2)$  is of the order of unity at the LHC and of the order of several units at the RHIC energies, the corresponding suppression of hard diffraction is very large because in the absence of the suppression, nuclear diffractive PDFs are enhanced compared to the nucleon diffractive PDFs by the impulse approximation factor  $f_{j/A}^{D(3)}/f_{j/N}^{D(3)} \propto A^{4/3}$ .

Figure 4 presents the  $A$ -dependence of  $\lambda^j$  at  $x = 10^{-3}$ , i.e. at fixed  $\sigma_{\text{eff}}^j$ . As seen from Fig. 4, the  $A$ -dependence of  $\lambda^j$  is rather slow. A simple fit gives that  $\lambda^j \propto A^{0.29}$  at the LHC and  $\lambda^j \propto A^{0.35}$  at RHIC.

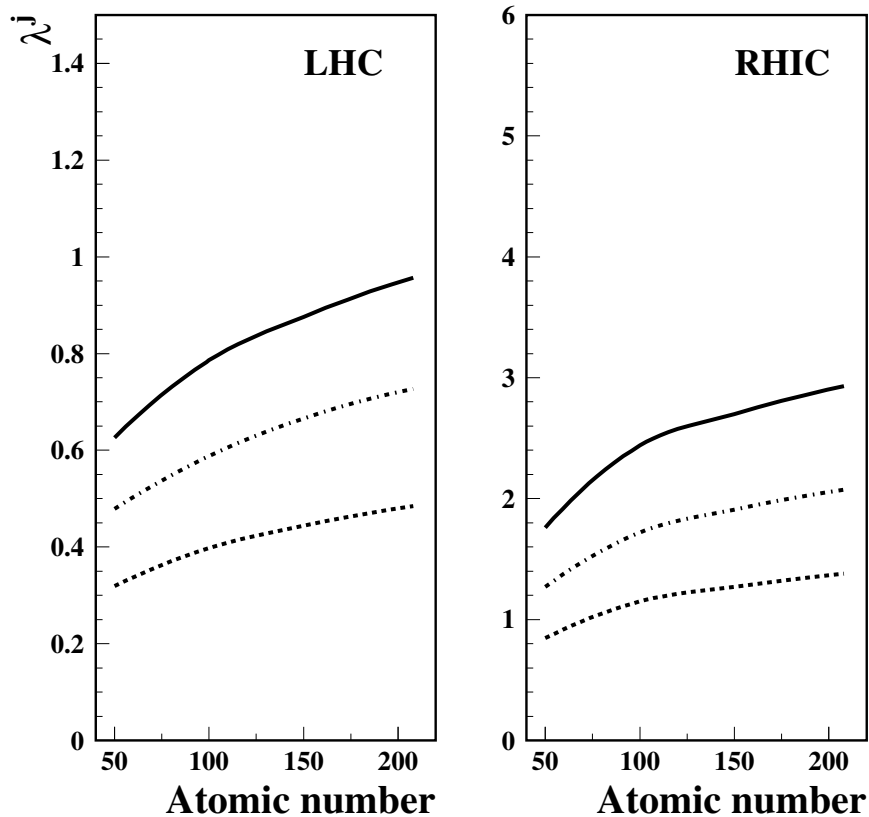


FIG. 4: The suppression factor  $\lambda^j$  of Eq. (12) as a function of the atomic number at  $x = 10^{-3}$  and at  $Q^2 = 4 \text{ GeV}^2$  in the LHC ( $\sqrt{s} \approx 9 \text{ TeV}$  but changes with  $A$ ) and RHIC ( $\sqrt{s} = 200 \text{ GeV}$ ) kinematics. The labeling of the curves is the same as in Fig. 3.

### III. HARD DIFFRACTION IN PA AND ULTRAPERIPHERAL COLLISIONS

We demonstrated in [13] that for  $pPb$  scattering at the LHC, most of the diffractive events ( $\sim 80\%$ ) will be generated via scattering of the proton off the coherent nuclear Coulomb field at large impact parameters. These ultraperipheral proton-nucleus collisions open a possibility for studies of hard photon-proton interactions at extremely high energies and allow to probe the gluon density in nucleons at the values of Bjorken  $x$  which are a factor of ten smaller (for the same virtuality) than those probed at HERA [18].

In this Section, we estimate the ratio of hard jet production due to the hard diffraction interactions in coherent  $pA$  scattering and due to the electromagnetic interactions. Qualita-

tively, we expect that the ratio will be rather small because of the following two suppression effects.

First, hard diffractive two-jet production is suppressed by the factor discussed in Sect. II. Second, the shapes of the parton distribution in the photon and in a screened nuclear diffractive PDFs are rather different. In the photon case, the dominant contribution to photon PDFs comes from  $\beta \sim 1$  corresponding to the kinematics where a pair of jets is at the rapidities close to the gap. On the other hand, in the screened nuclear diffractive PDFs at large virtualities, which are relevant for the measurements at the LHC, the main contribution comes from small  $\beta$ , see Fig. 3 of [10].

For a quantitative analysis of the discussed ratio, we used the leading order approximation for diffractive two-jet production. The hard diffractive two-jet cross section can be readily obtained by generalizing the well-known expression for the two-jet inclusive cross section in hadron-hadron scattering [19]

$$\begin{aligned} \frac{d^3\sigma}{dx_1 dp_T^2 dx_{IP}} &\propto \sum_{i,j,k,l=q,\bar{q},g} f_{i/p}(x_1, Q_{\text{eff}}^2) \tilde{f}_{j/A}^{D(3)}(\beta, x_{IP}, Q_{\text{eff}}^2) \overline{\sum} |\mathcal{M}(ij \rightarrow kl)|^2 \frac{1}{1 + \delta_{kl}} \\ &\propto r_h \sum_{i,j,k,l=q,\bar{q},g} f_{i/p}(x_1, Q_{\text{eff}}^2) \lambda^j(\beta x_{IP}, Q_{\text{eff}}^2) f_{j/N}^{D(3)}(\beta, x_{IP}, Q_{\text{eff}}^2) \overline{\sum} |\mathcal{M}(ij \rightarrow kl)|^2 \frac{1}{1 + \delta_{kl}}, \end{aligned} \quad (13)$$

where  $f_{i/p}$  are the projectile PDFs;  $\tilde{f}_{j/A}^{D(3)}$  are the screened nuclear diffractive PDFs;  $\overline{\sum} |\mathcal{M}(ij \rightarrow kl)|^2$  are invariant matrix elements for two-to-two parton scattering given in Table 7.1 of [19]. In the second line, we used that [see Eq. (12)]

$$\tilde{f}_{j/A}^{D(3)} = \lambda^j \tilde{f}_{j/N}^{D(3)} = \lambda^j r_h f_{j/N}^{D(3)}. \quad (14)$$

It is important to note that in Eqs. (13) and (14) we introduced the suppression factor  $r_h$ , which takes into account significant factorization breaking in hard hadron-hadron diffraction. In our numerical analysis, we use the phenomenological model of [5], which describes the suppression of diffraction at the CDF ( $\sqrt{s} = 546$  and 1800 GeV) by rescaling the Pomeron flux

$$r_h = \frac{1}{N(s)} = \left( \int_{x_{IP,\min}}^{x_{IP,\max}} dx_{IP} \int_{-\infty}^0 dt f_{IP/p}(x_{IP}, t) \right)^{-1}, \quad (15)$$

where  $f_{IP/p}(x_{IP}, t)$  is the Pomeron flux;  $x_{IP,\max} = 0.1$  and  $x_{IP,\min} = 1.5/s$ . The application of Eq. (15) at the RHIC and LHC energies gives

$$\begin{aligned} r_h &= \frac{1}{3.33} && \text{RHIC}, \\ r_h &= \frac{1}{12.79} && \text{LHC}. \end{aligned} \quad (16)$$

In our analysis we need the suppression factor at  $t = 0$  (since the elementary diffractive amplitude enters Eq. (4) at  $t = 0$ ), while experimentally the suppression factor was estimates using the  $t$ -integrated cross section. In order to take into account the increase of the suppression factor at  $t = 0$  (small impact parameters, which are responsible for the factorization breaking, are more important in the differential cross section at  $t = 0$  than in the  $t$ -integrated cross section), we increase the suppression factors of Eq. (16) by 25%. The suppression factors that we use in our numerical estimates are then

$$\begin{aligned} r_h &= \frac{1}{4.2} & \text{RHIC,} \\ r_h &= \frac{1}{16.0} & \text{LHC.} \end{aligned} \quad (17)$$

Note that the suppression factors  $r_h$  are assumed to be  $x_{IP}$ -independent [5].

Another important parameter, which affects the  $x_{IP}$ -dependence of the Pomeron flux, is the deviation of the Pomeron intercept from unity,  $\epsilon = \alpha_{IP}(0) - 1$ ,

$$f_{IP/p}(x_{IP}) = \frac{1}{x_{IP}^{1+2\epsilon}} \int_{-\infty}^0 dt \frac{e^{b_0 t}}{x_{IP}^{2\alpha' t}}, \quad (18)$$

where  $b_0 = 4.6 \text{ GeV}^{-2}$  and  $\alpha' = 0.25 \text{ GeV}^{-2}$ . For the nucleon diffractive PDFs  $f_{j/N}^{D(3)}$ , we use the H1 fit to the HERA data on hard diffraction at  $\sqrt{s} \approx 300 \text{ GeV}$  [23], which corresponds to  $\epsilon = 0.203 \pm 0.020 \pm 0.013$ . On the other hand, the data on hard proton-antiproton diffraction at Fermilab at  $\sqrt{s} \approx 546$  and  $1800 \text{ GeV}$  can be described by the renormalized Pomeron flux [see Eq. (15)] calculated with  $\epsilon = 0.1$ . Therefore, it appears that in order to properly take into account the breaking of factorization in hadron-hadron scattering, along with the factor  $r_h$ , one needs to use the Pomeron flux with  $\epsilon \approx 0.1$ . In our numerical analysis, we make predictions using both  $\epsilon = 0.2$  and  $\epsilon = 0.1$  values.

For the simplification of the analysis, we assumed that the light-cone fraction  $x_1$ , the jet transverse momentum  $p_T$  and the nuclear light-cone fraction loss  $x_{IP}$  are known. In addition, we consider only the case of  $90^\circ$  hard parton scattering in the center of mass, which constrains  $x_1$  (as a function of  $x_2 = \beta x_{IP}$ ) and  $Q_{\text{eff}}^2$

$$x_1 = \frac{4 p_T^2}{\beta x_{IP} s}, \quad Q_{\text{eff}}^2 = 4 p_T^2, \quad (19)$$

where  $\sqrt{s}$  is the proton-nucleon invariant energy.

For coherent two-jet production, which takes place via the e.m. mechanism (the nucleus coherently emits a quasi-real photon which interacts with the proton and diffractively produces two hard jets), the corresponding cross section can be written in a similar form as a

sum of the resolved and direct photon contributions (the separation into the resolved and direct components is only meaningful in the leading-order calculation)

$$\begin{aligned} \frac{d^3\sigma^{\text{e.m.}}}{dx_1 dp_T^2 dx_{IP}} &\propto r_{\text{e.m.}} \sum_{i,j,k,l=q,\bar{q},g} f_{i/p}(x_1, Q_{\text{eff}}^2) \frac{n(x_{IP})}{x_{IP}} f_{j/\gamma}(\beta, Q_{\text{eff}}^2) \overline{\sum} |\mathcal{M}(ij \rightarrow kl)|^2 \frac{1}{1 + \delta_{kl}} \\ &+ \sum_{i,j,k,l=q,\bar{q},g} f_{i/p}(x_1, Q_{\text{eff}}^2) \frac{n(x_{IP})}{x_{IP}} \delta(\beta - 1) \overline{\sum} |\mathcal{M}(i\gamma \rightarrow kl)|^2 \frac{1}{1 + \delta_{kl}}, \end{aligned} \quad (20)$$

where  $n(x_{IP})$  is the flux of equivalent photons [22] expressed in terms of  $x_{IP}$  instead of the photon energy  $\omega$  (note the factor  $1/x_{IP}$  coming from the  $1/\omega$  in the spectrum of the equivalent photons);  $f_{j/\gamma}$  is the PDF of the real photon;  $\overline{\sum} |\mathcal{M}(i\gamma \rightarrow kl)|^2$  are invariant matrix elements for the direct photon-parton scattering, see Table 7.9 in [19];  $r_{\text{e.m.}}$  is a phenomenological factor describing the factorization breaking for the resolved (hadron-like) component of the real photon. The exact value of  $r_{\text{e.m.}}$  is uncertain: it ranges from  $r_{\text{e.m.}} = 0.34$  [20] to  $r_{\text{e.m.}} \approx 1$  with large errors [21]. Since our analysis is a simple LO estimate, we conservatively take  $r_{\text{e.m.}} = 0.5$ .

The flux of the equivalent photons approximately equals [22]

$$n(x_{IP}) \approx \frac{2Z^2 \alpha_{\text{e.m.}}}{\pi} \ln \left( \frac{\gamma}{R_A x_{IP} p_{\text{lab}}} \right), \quad (21)$$

where  $Z$  is the nuclear charge;  $\gamma$  is the Lorentz factor ( $\gamma \approx 3000$  for  $pPb$  at the LHC [15]);  $R_A = 1.145 A^{1/3}$  is the nuclear effective radius;  $p_{\text{lab}}$  is the momentum of the nucleus in the laboratory frame ( $p_{\text{lab}} \approx 2.75$  TeV for  $pPb$  at the LHC). In practice, we used a more precise formula for the flux of the equivalent photons, which reduces the result of Eq. (21) by 11% [24].

We are now ready to estimate the ratio of the hard diffractive two-jet cross section to the e.m. two-jet cross section,  $R$ ,

$$R(\beta, x_{IP}, p_T) = \frac{d^3\sigma}{dx_1 dp_T^2 dx_{IP}} \Big/ \frac{d^3\sigma^{\text{e.m.}}}{dx_1 dp_T^2 dx_{IP}}, \quad (22)$$

where the involved cross section are given by Eqs. (13) and (20) with equal coefficients of proportionality. In the simplified kinematics that we use, at given  $p_T$  and  $x_{IP}$ , the ratio  $R$  depends only on  $\beta$ .

We considered two cases: two-jet production summing over production of gluon and quark jets and production of two heavy quark jets. The resulting  $R$  ratios at  $p_T = 5$  GeV and  $x_{IP} = 10^{-4}, 10^{-3}$  and  $10^{-2}$  as functions of  $\beta$  are presented in Figs. 5 and 6, respectively. In

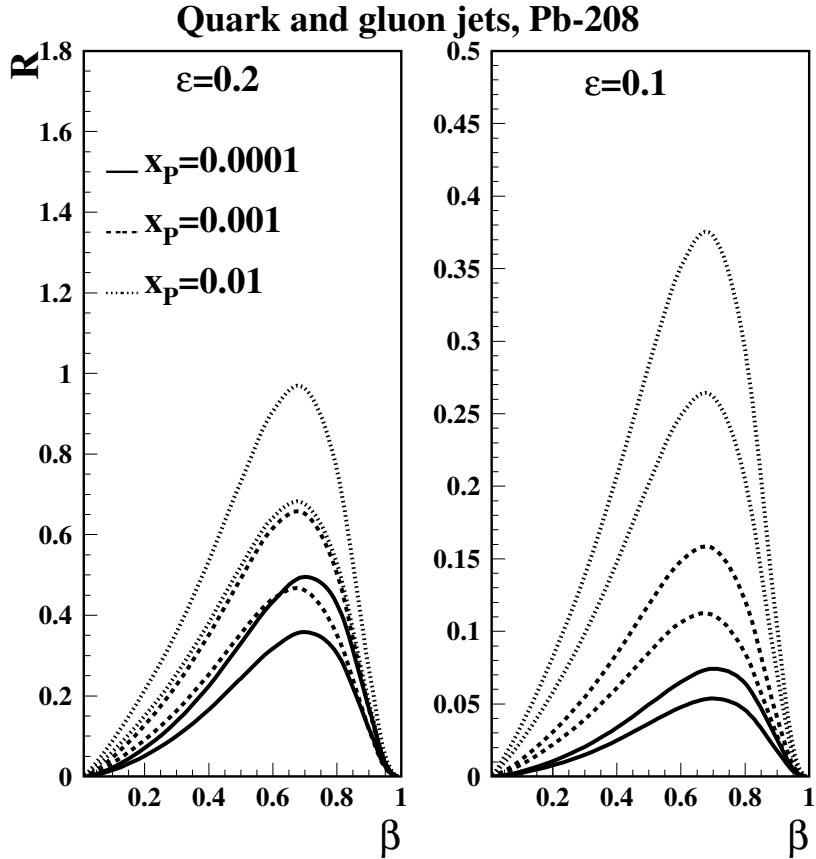


FIG. 5: The suppression of hard diffractive two-jet (quark and gluon jets) production compared to e.m. coherent two-jet production in proton-Pb scattering. The suppression factor  $R$  is given by Eq. (22) and is evaluated at  $p_T = 5$  GeV and  $x_{IP} = 10^{-4}$ ,  $10^{-3}$  and  $10^{-2}$  as a function of  $\beta$ . The two sets of curves correspond to two scenarios of the suppression of the nuclear gluon diffractive PDF, see Fig. 3. The left panel corresponds to the calculation using the Pomeron flux with  $\epsilon = 0.2$ ; the right panel corresponds to  $\epsilon = 0.1$ .

Fig. 5, we give two sets of curves, which correspond to the two scenarios of nuclear shadowing of the nuclear gluon diffractive PDF, see Fig. 3. Since the role of the gluons is negligible in Fig. 6, there is one set of curves depending on nuclear shadowing in the sea quark channel.

The results presented in Figs. 5 and 6 deserve a detailed discussion. The dependence of the ratio  $R$  on  $x_{IP}$  is not strong and can be explained by the fact that  $f_{j/N}^{D(3)}(\beta, x_{IP}, Q_{\text{eff}}^2) \propto 1/x_{IP}^{1+2\epsilon}$ , see Eq. (18), which is only slightly faster than the  $1/x_{IP} \ln(1/x_{IP})$  behavior of the e.m. cross section. On the other hand, the main contribution to the  $x_{IP}$ -dependence at fixed

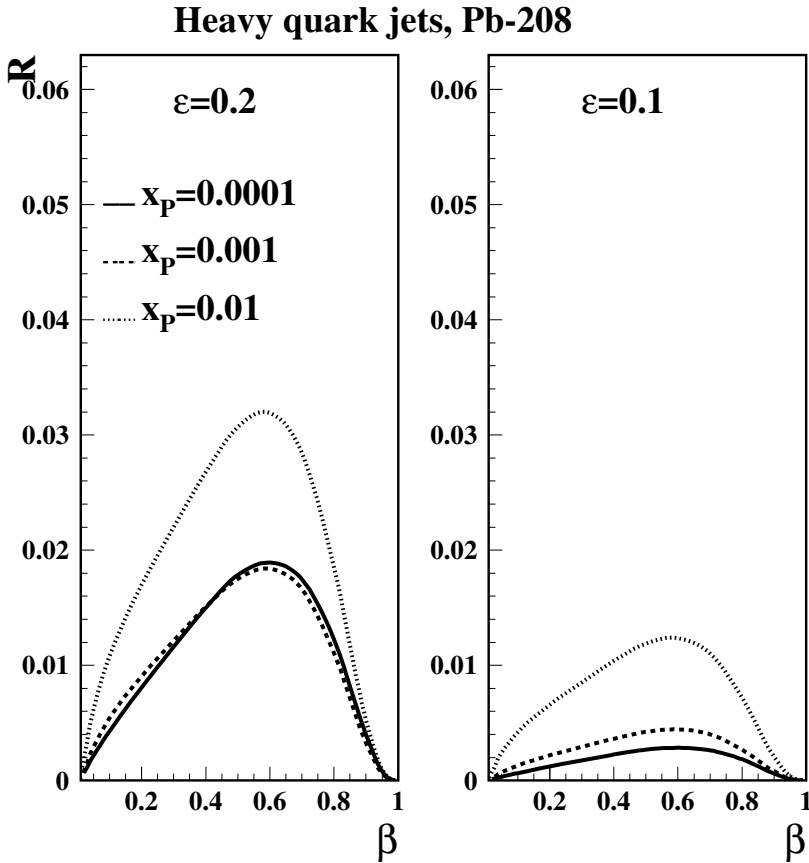


FIG. 6: The suppression of hard diffractive heavy quark two-jet production compared to e.m. coherent two-jet production in proton-Pb scattering. The suppression factor  $R$  is given by Eq. (22) and is evaluated at  $p_T = 5$  GeV and  $x_{IP} = 10^{-4}, 10^{-3}$  and  $10^{-2}$  as a function of  $\beta$ .

$\beta$  comes from the changing  $x_1$ . As  $x_{IP}$  is decreased,  $x_1$  is increased, which diminishes the role played by gluons in the projectile. As explained in the following, it is the gluon contribution that increases  $R$ . Hence,  $R$  decreases with decreasing  $x_{IP}$ .

The dependence of  $R$  on  $\beta$  is much faster and reflects different shapes of diffractive PDFs of the proton and PDFs of the real photon. While the diffractive PDFs times  $\beta$  are flat in the  $\beta \rightarrow 0$  limit, the photon PDFs times  $\beta$  grow. This explains why  $R$  approaches zero when  $\beta$  is small. In the opposite limit,  $\beta \rightarrow 1$ , diffractive PDFs vanish and the e.m. contribution wins over due to the direct photon contribution existing at  $b \approx 1$ :  $R \rightarrow 0$  as  $\beta \rightarrow 1$ .

In Fig. 5, the ratio  $R$  at its peak is as large as unity, which is large and unexpected. An examination shows that this effect is due to the large gluon diffractive PDF [23], which in

tandem with the large  $gg \rightarrow gg$  hard parton invariant matrix element [19], works to increase  $R$ .

The effect of gluons is reduced to almost nil, when we consider production of two heavy quark jets. The ratio  $R$  immediately and expectedly reduced to a few percent level, see Fig. 6.

In our numerical analysis of the ratio  $R$ , we used the LO parameterization of the real photon PDFs from [25]. We have also checked that the use of a different parameterization [26] leads to rather similar predictions.

For the nucleon diffractive PDFs, we used the H1 fit [23]. The  $\lambda^j(x, Q^2)$  suppression factor, which enters Eq. (22) at the scale  $Q^2 = Q_{\text{eff}}^2 = 100 \text{ GeV}^2$ , was evaluated using Eq. (12) with  $\sigma_{\text{eff}}^j(x, Q^2)$  at the same  $Q^2 = Q_{\text{eff}}^2 = 100 \text{ GeV}^2$  scale, see Eq. (3).

The  $\delta$ -function for the direct photon contribution was numerically modeled in the following simple form

$$\delta(\beta - 1) = \frac{1}{\pi} \frac{\epsilon}{(\beta - 1)^2 + \epsilon^2}, \quad \text{with } \epsilon = 0.01. \quad (23)$$

It is instructive to examine how our predictions for the suppression factor  $R$  change, when the heavy nucleus of  $^{208}\text{Pb}$  is replaced by a lighter nucleus of  $^{40}\text{Ca}$ . Note that for  $p\text{Ca}$  scattering at the LHC,  $\sqrt{s} = 9.9 \text{ TeV}$  and  $\gamma \approx 3700$  [15]. We expect that the ratio  $R$  will significantly increase because of the reduction of the flux of the equivalent photons (the flux is proportional  $Z^2$ ). Figure 7 presents the ratio  $R$  for  $^{40}\text{Ca}$ . The labeling of the curves is the same as in Figs. 5 and 6. As can be seen from the comparison of Fig. 7 to Figs. 5 and 6, the ratio  $R$  scales by the factor  $\approx 10$  for  $x_{IP} = 10^{-4}$  and  $10^{-3}$  and by the factor  $\approx 5$  at  $x_{IP} = 10^{-2}$ , when going from  $^{208}\text{Pb}$  to  $^{40}\text{Ca}$ .

Besides the LHC, RHIC has also a potential to measure hard diffraction in proton-nucleus scattering. We consider a typical example of the corresponding RHIC kinematics with 250 GeV protons scattering on 100 GeV/per nucleon nuclei (the corresponding  $\sqrt{s} \approx 320 \text{ GeV}$  and the Lorentz dilation factor is  $\gamma \approx 100$ ). Producing sufficiently high diffractive masses, e.g.  $M_X^2 = 500 \text{ GeV}^2$ , one accesses the typical kinematics of hard diffraction,  $x_{IP} = 5 \times 10^{-3}$  and  $\beta > 0.3$ . Note also that the suppression of hard diffraction at RHIC is approximately four times smaller than at the LHC, see Eq. (17).

We studied the suppression factor  $R$  of Eq. (22) in the considered RHIC kinematics at  $p_T = 5 \text{ GeV}$ . The resulting values of  $R$  as a function of  $\beta$  are presented in Fig. 8. The solid curves correspond to quark and gluon jets; the dotted curves correspond to heavy quark

jets. The two sets of solid curves correspond to the two scenarios of the suppression of the nuclear gluon diffractive PDF, see Fig. 3.

As seen from Fig. 8, the factor  $R$  is similar in the RHIC and LHC kinematics. Two effects work in the opposite directions and make the suppression at RHIC similar to the LHC. The smaller value of  $\gamma$  decreases the flux of the equivalent photons and works to increase  $R$ . At the same time, the smaller  $\sqrt{s}$  at RHIC means larger values of  $x_1$ , which decreases the role of gluons. This effect decreases  $R$  such that the two effects almost compensate each other.

#### IV. CONCLUSIONS

Using the leading twist theory of nuclear shadowing, we developed a method for the calculation of coherent hard diffraction processes off nuclei. We showed that soft multiple rescatterings lead to the factorization breaking of hard diffraction in proton-nucleus scattering, which is larger than the well-known factorization breaking of diffraction in hadron-nucleon scattering.

Based on these results, we compare the contribution of hard diffraction into two jets to the e.m. contribution, when the two-jet diffractive final state is produced by the coherent nuclear Coulomb field. We study the  $x_P$ ,  $\beta$  and  $A$ -dependence of the ratio of the two effects,  $R$ , at the LHC and RHIC kinematics. In addition, we separately study the case when the final jets consist of quarks and gluons and the case when the final jets consist of heavy ( $c$  and  $b$ ) quarks. We find that  $R$  is sensitive to the value of the Pomeron intercept: changing  $\epsilon$  from 0.2 to 0.1 reduces the Pomeron flux by the factor  $\approx 3$  in the considered kinematics and, hence, leads to the corresponding decrease of  $R$ .

Our results can summarized as follows. For proton-Pb scattering at the LHC, hard diffraction is suppressed compared to the e.m. contribution, especially at  $x_P = 10^{-4}$  and large  $\beta$ , e.g.  $\beta > 0.8$ . The suppression is very strong for the production of heavy quark jets:  $R$  is at the level of few per cent. The physical reason of the suppression is the strong coherent Coulomb field of  $^{208}\text{Pb}$ , which enhances the e.m. mechanism of hard diffraction.

Replacing  $^{208}\text{Pb}$  by  $^{40}\text{Ca}$ , the hard diffractive mechanism becomes compatible to the e.m. one. The suppression becomes more strongly dependent on  $\epsilon$  and is not so dramatic for the heavy quark jets.

As a result of the compensation between the lower values of  $\sqrt{s}$  and the Lorentz dilation

factor  $\gamma$  at RHIC, the suppression factor  $R$  at the RHIC kinematics is very similar to  $R$  at the LHC.

Our results suggest the following experimental strategies. First, the use of heavy nuclei in  $pA$  scattering at the LHC will provide a clean method to study hard photon-proton scattering at the energies exceeding the HERA energies by the factor of 10. Second, taking lighter nuclei and choosing the appropriate kinematics, where the e.m. contribution is small, one can effectively study the factorization breaking in nuclear diffractive PDFs. Third, in the same kinematics, a comparison of the dijet diffractive production to the heavy-quark-jet diffractive production will measure the nuclear screened diffractive gluon PDF. It can be compared to the nuclear diffractive PDFs, which will be measured in nucleus-nucleus ultraperipheral collisions at the LHC.

### Acknowledgements

We would like to thank K. Goulianos for valuable discussions of the factorization breaking in  $p\bar{p}$  diffraction and M. Zhalov for the discussions of the suppression factor for hard diffraction and the calculation of the correction to the flux of equivalent photons. This work is supported by the Sofia Kovalevskaya Program of the Alexander von Humboldt Foundation (Germany) and DOE (USA). M.S. thanks the Frankfurt Institute for Advanced Studies at Frankfurt University for the hospitality during the time when this work was completed.

- 
- [1] R. Bonino *et al.* [UA8 Collaboration], Phys. Lett. B **211** (1988) 239.
  - [2] H. Abramowicz and A. Caldwell, Rev. Mod. Phys. **71** (1999) 1275 [arXiv:hep-ex/9903037].
  - [3] J. C. Collins, Phys. Rev. D **57** (1998) 3051 [Erratum-ibid. D **61** (2000) 019902] [arXiv:hep-ph/9709499].
  - [4] K. Goulianos, arXiv:hep-ph/0407035.
  - [5] K. Goulianos, Phys. Lett. B **358** (1995) 379.
  - [6] A. B. Kaidalov, V. A. Khoze, A. D. Martin and M. G. Ryskin, Acta Phys. Polon. B **34** (2003) 3163 [arXiv:hep-ph/0303111].
  - [7] L. Frankfurt, M. Strikman, C. Weiss and M. Zhalov, arXiv:hep-ph/0412260.

- [8] L. Frankfurt and M. Strikman, Eur. Phys. J. A **5** (1999) 293 [arXiv:hep-ph/9812322].
- [9] L. Frankfurt, V. Guzey and M. Strikman, Phys. Rev. D **71** (2005) 054001 [arXiv:hep-ph/0303022].
- [10] L. Frankfurt, V. Guzey and M. Strikman, Phys. Lett. B **586** (2004) 41 [arXiv:hep-ph/0308189].
- [11] L. Frankfurt, G. A. Miller and M. Strikman, Phys. Rev. Lett. **71** (1993) 2859 [arXiv:hep-ph/9309285].
- [12] L. Frankfurt, V. Guzey and M. Strikman, J. Phys. G **27** (2001) R23 [arXiv:hep-ph/0010248].
- [13] V. Guzey and M. Strikman, arXiv:hep-ph/0505088.
- [14] K. S. Kolbig and B. Margolis, Nucl. Phys. B **6** (1968) 85.
- [15] A. Morsch, in *Hard probes in heavy-ion collisions at the LHC*, Eds. M. Mangano, H. Satz and U. Wiedemann, report CERN-2004-009, CERN, 2004.
- [16] F. Abe *et al.* [CDF Collaboration], Phys. Rev. D **50** (1994) 5535.
- [17] A. Donnachie and P. V. Landshoff, Phys. Lett. B **296** (1992) 227 [arXiv:hep-ph/9209205].
- [18] M. Strikman, R. Vogt, and S. White, in preparation.
- [19] R.K. Ellis, W.J. Stirling and B.R. Webber, *QCD and Collider Physics*, Cambridge Univ. Press, 1996, p. 248.
- [20] M. Klasen and G. Kramer, Phys. Rev. Lett. **93** (2004) 232002 [arXiv:hep-ph/0410105].
- [21] S. Chekanov *et al.* [ZEUS Collaboration], Eur. Phys. J. C **23** (2002) 615 [arXiv:hep-ex/0112029].
- [22] G. Baur, K. Hencken, D. Trautmann, S. Sadovsky and Y. Kharlov, Phys. Rept. **364** (2002) 359 [arXiv:hep-ph/0112211].
- [23] C. Adloff *et al.* [H1 Collaboration], Z. Phys. C **76** (1997) 613 [arXiv:hep-ex/9708016].
- [24] M. Zhalov, private communication.
- [25] M. Gluck, E. Reya and A. Vogt, Phys. Rev. D **46** (1992) 1973.
- [26] H. Abramowicz, K. Charchula and A. Levy, Phys. Lett. B **269** (1991) 458.

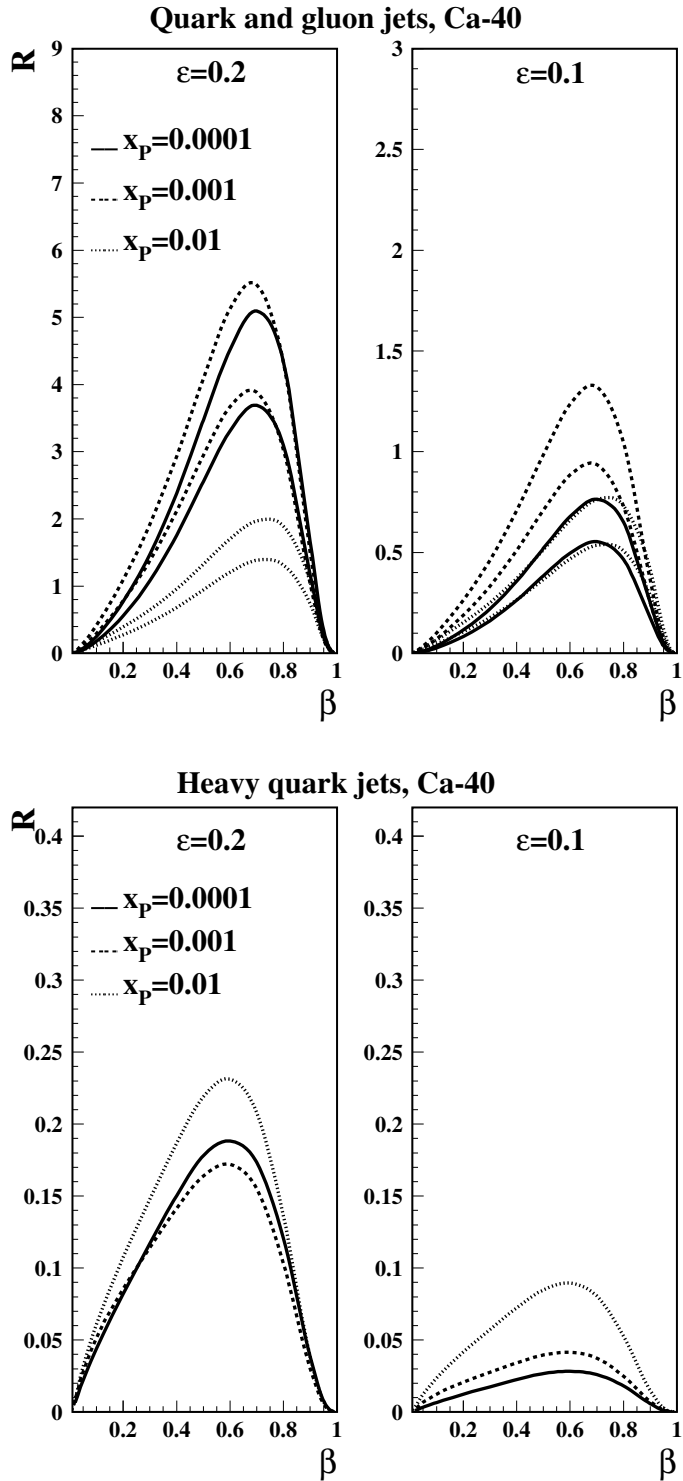


FIG. 7: The suppression of hard diffractive two-jet production compared to e.m. coherent two-jet production in proton-Ca scattering. The suppression factor  $R$  of Eq. (22) is evaluated at  $p_T = 5$  GeV and  $x_P = 10^{-4}, 10^{-3}$  and  $10^{-2}$  as a function of  $\beta$ . The two sets of curves in the upper panels correspond to the two scenarios of suppression of the nuclear gluon diffractive PDF, see Fig. 3.

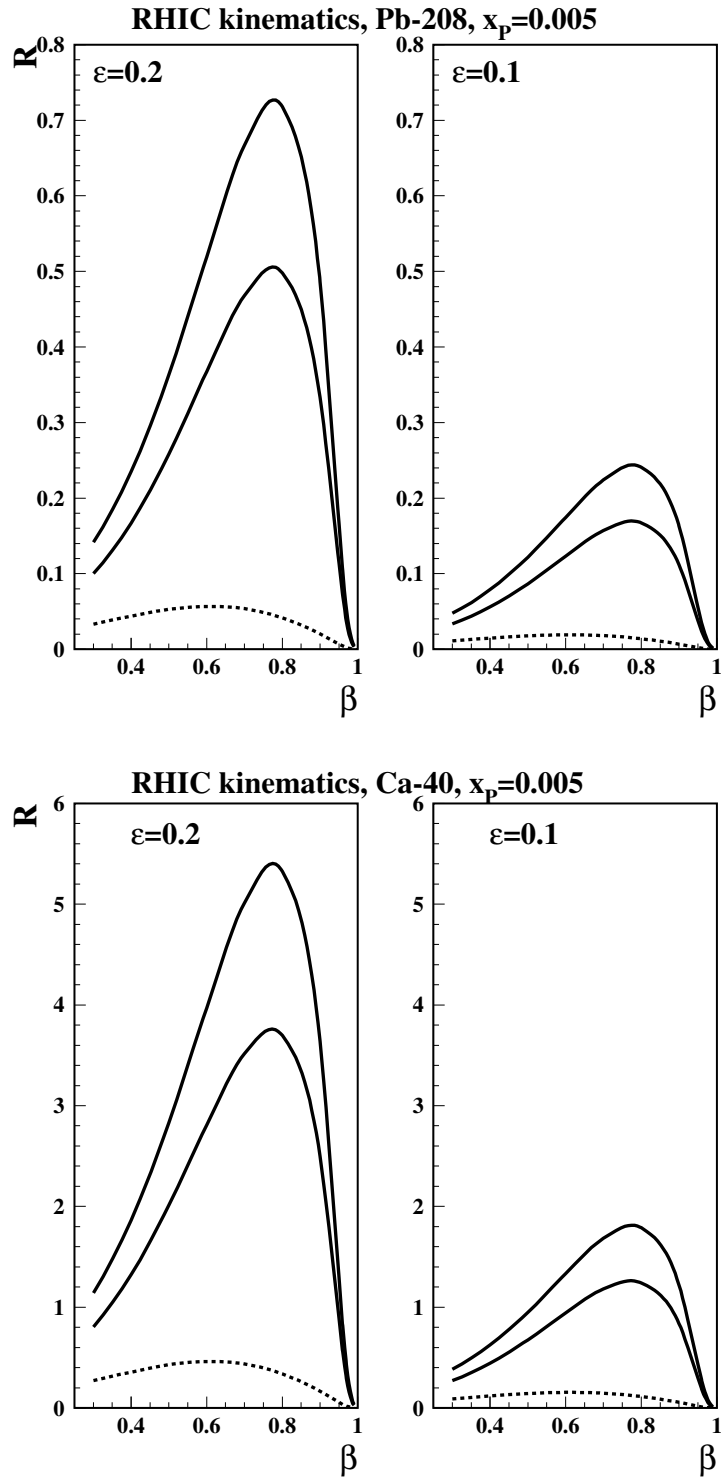


FIG. 8: The suppression factor  $R$  of Eq. (22) in the RHIC kinematics and at  $p_T = 5$  GeV and  $x_{IP} = 5 \times 10^{-3}$  as a function of  $\beta$ . The solid curves correspond to quark and gluon jets; the dotted curves correspond to heavy quark jets. The two solid curves correspond to the two scenarios of suppression of the nuclear gluon diffractive PDF.